Systematic study of longitudinal and transverse helicity amplitudes in the hypercentral constituent quark model

E. Santopinto
I.N.F.N., Sezione di Genova, Genova, Italy

M. M. Giannini
Dipartimento di Fisica dell'Università di Genova and I.N.F.N., Sezione di Genova, Genova, Italy

(Received 7 May 2012; revised manuscript received 26 July 2012; published 7 December 2012)

We report in a systematic way the predictions of the nonrelativistic hypercentral constituent quark model for the electromagnetic excitations of baryon resonances. The longitudinal and transverse helicity amplitudes are calculated with no free parameters for fourteen resonances, for both protons and neutrons. The calculations lead to an overall fair description of data, especially in the medium-Q^2 range, where quark degrees of freedom are expected to dominate.

DOI: 10.1103/PhysRevC.86.065202 PACS number(s): 12.39.Jh, 14.20.Gk, 13.40.Gp, 24.85.+p

I. INTRODUCTION

Various constituent quark models (CQMs) [1] have been proposed in the recent past after the pioneering work of Isgur and Karl (IK) [2]. Among them we quote the relativized Capstick-Isgur (CI) model [3], the algebraic approach (BIL) [4], the hypercentral CQM (hCQM) [5–7], the chiral Goldstone boson exchange model (GBE) [8,9], and the Bonn instanton model (BN) [10].

The ingredients of the models are quite different, but they have a simple general structure, since they can be split into a spin-flavor-independent part $V_{\rm inv}$, which is SU(6) invariant and contains the confinement interaction, and a SU(6)-dependent part V_{sf}, which contains spin and eventually flavor-dependent interactions, in agreement with the prescription provided by the early lattice QCD calculations [11]. For the latter, the hyperfine interaction is often used [12]. They are all able to reproduce the baryon spectrum, which is the first quantity to be described, but a real test of the models is provided by their systematic and consistent application to the description of other physical quantities of the nucleon. In this respect it is interesting to see to what extent and how systematically the various CQMs have been used; one should not forget that in many cases the calculations referred to as a CQM are actually performed using a simple harmonic oscillator (h.o.) wave function for the internal quark motion in either a nonrelativistic (HO) or relativistic (rHO) framework.

The photocouplings for the excitation of the baryon resonances have been calculated in various models; among others, we quote HO [13], IK [14], CI [15], BIL [4], and hCQM [16] (for a comparison among these and other approaches, see, e.g., Refs. [16,17]). The calculations are in general able to reproduce the overall trend, but the strength is systematically less than the data; such similarity of results coming from quite different models can be ascribed to the common SU(6) structure quoted above.

In many cases the models have been applied to the description of the elastic nucleon form factors. The algebraic method of BIL [4,18] has been used, assuming a definite charge distribution along the string connecting quarks, while the CI model is the basis of a light front calculation by the Rome group [19] and gives a good description of data, provided that quark form factors are introduced. The hCQM has been first applied in the nonrelativistic version with Lorentz boosts [20,21], showing that the recently observed [22] behavior of the ratio between the charge and magnetic form factors of the proton may be ascribed to relativistic effects; the hCQM has been reformulated relativistically in a point form approach, and the resulting elastic nucleon form factors are quite good and further improved by the introduction of intrinsic quark form factors [23,24]. A good description of the elastic form factors is achieved also using the GBE [25,26] and the BN [27] models, both being fully relativistic.

The calculation of the elastic form factors allows to understand to what extent the ground state is under control, whereas the study of the Q^2 behavior of the excitation to the baryon resonances provides a sensible test of both the energy and the short-range properties of the quark structure. This fact motivates the attention that has been devoted to the electromagnetic transition form factors (helicity amplitudes).

In the HO framework, there are various calculations of the transverse helicity amplitudes; among them we quote Refs. [13,14,28–30], while a systematic rHO approach has been used by Ref. [31]. A light cone calculation, using the CI [3] model, has been successfully applied to the Δ [32] and Roper excitation [33]. For more recent light cone approaches, see Ref. [34] and references therein. The algebraic method, with the assumed charge distribution of the string, has been also used for the calculation of the transverse helicity amplitudes. The hCQM, in its nonrelativistic version, leads to nice predictions for the transverse excitation of the negative parity resonances [35]. In both cases the theoretical curves exhibit depletion at low Q^2, which is consistent with the results for the photocouplings.

A systematic description of the helicity amplitudes is still lacking. In this paper we present the *predictions* of the nonrelativistic hCQM [5] for the longitudinal and transverse form factors for the excitation of fourteen baryon resonances, in comparison with the most recent experimental data. The

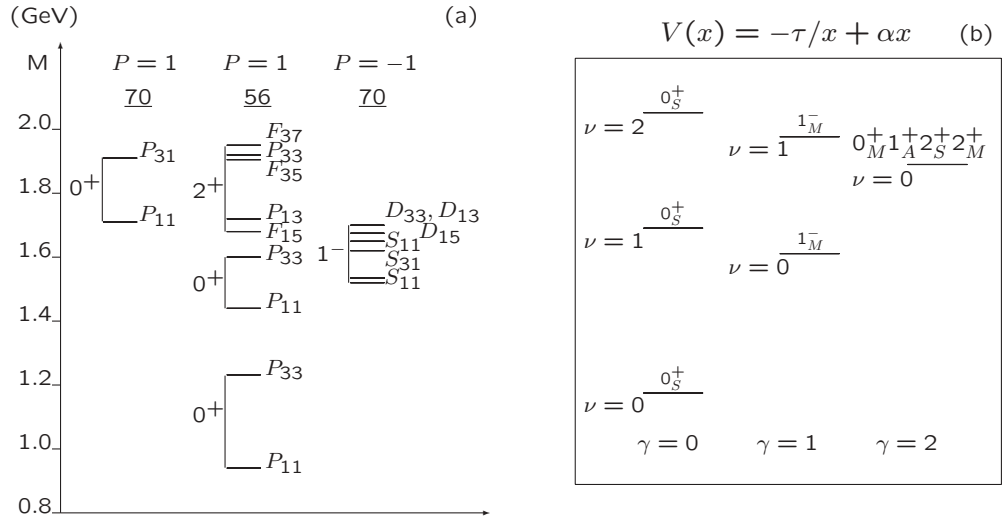

FIG. 1. (a) The experimental spectrum of the nonstrange three- and four-star resonances [38]. The states are reported in columns with the same parity P and grouped into SU(6) multiplets. (b) The spectrum given by the SU(6)-invariant part of the Hamiltonian Eq. (9).

curves for the transverse excitation of the negative-parity resonances have been already published in Ref. [35], but we report them here also since in the past years new data have been published. Some of the remaining curves have been presented at various conferences [36].

II. THE HYPERCENTRAL MODEL

We review briefly the hypercentral CQM, introduced in Ref. [5], where the free parameters of the quark interaction have been fixed in order to describe the nonstrange baryon spectrum. The same parameters have been used for the calculation of various quantities (photocouplings [16], transverse helicity amplitudes for the excitation of negative parity resonances [35], and elastic nucleon form factors [21,37]). These parameters are used for the present calculation of the longitudinal and transverse helicity amplitudes.

The four- and three-star [38] nonstrange resonances can be arranged in SU(6) multiplets, indicating that the quark dynamics has a dominant SU(6) invariant part that accounts for the average multiplet energies [see Fig. 1(a)]. The splittings within the multiplets are obtained by means of a SU(6) violating interaction, which can be spin and/or isospin dependent and can be treated as a perturbation.

After removal of the center-of-mass coordinate, the space configurations of three quarks in the nonstrange baryons are described by the Jacobi coordinates, $\vec{\rho}$ and $\vec{\lambda}$,

$$\vec{\rho} = \frac{1}{\sqrt{2}}(\vec{r}_1 - \vec{r}_2), \quad \vec{\lambda} = \frac{1}{\sqrt{6}}(\vec{r}_1 + \vec{r}_2 - 2\vec{r}_3). \tag{1}$$

One can introduce the hyperspherical coordinates, which are obtained by substituting $\rho = |\vec{\rho}|$ and $\lambda = |\vec{\lambda}|$ with the hyperradius, x, and the hyperangle, ξ, defined respectively by

$$x = \sqrt{\vec{\rho}^2 + \vec{\lambda}^2}, \quad \xi = \mathrm{arctg}\left(\frac{\rho}{\lambda}\right). \tag{2}$$

Using these coordinates, the kinetic term in the three-body Schrödinger equation can be rewritten as [39]

$$-\frac{1}{2m}(\Delta_\rho + \Delta_\lambda) = -\frac{1}{2m}\left(\frac{\partial^2}{\partial x^2} + \frac{5}{x}\frac{\partial}{\partial x} - \frac{L^2(\Omega_\rho, \Omega_\lambda, \xi)}{x^2}\right). \tag{3}$$

where $L^2(\Omega_\rho, \Omega_\lambda, \xi)$ is the six-dimensional generalization of the squared angular momentum operator. Its eigenfunctions are the well-known hyperspherical harmonics [39] $Y_{[\gamma]l_\rho l_\lambda}(\Omega_\rho, \Omega_\lambda, \xi)$ having eigenvalues $\gamma(\gamma+4)$, with $\gamma = 2n + l_\rho + l_\lambda$ (n is a non-negative integer); they can be expressed as products of standard spherical harmonics and Jacobi polynomials.

In the hCQM [5], the SU(6) invariant quark interaction is assumed to depend on the hyper-radius x only $V_{\mathrm{inv}} = V_{3q}(x)$. It has been observed that a two-body quark-quark potential leads to matrix elements in the baryon space quite similar to those of a hypercentral potential [40]. On the other hand, a two-body potential that is treated in the hypercentral approximation [41] and averaged over angles and hyperangle, is transformed into a potential that depends on x only; in particular, a power-like two-body potential $\sum_{i<j}(r_{ij})^n$ in the hypercentral approximation is given by a term proportional to x^n. The hypercentral approximation has been shown to be valid, since it provides a good description of baryon dynamics, especially for the lower states [41].

The hyper-radius x is a function of the coordinates of all the three quarks and $V_{3q}(x)$ has also a three-body character. There are many reasons supporting the idea of considering three-body interactions. First of all, three-body mechanisms are certainly generated by the fundamental multigluon vertices predicted by QCD; however, their explicit treatment is not possible with the present theoretical approaches and the presence of three-body mechanisms in quark dynamics can be simply viewed as "QCD inspired." Furthermore, flux

tube models, which have been proposed as a QCD-based description of quark interactions [42], lead to Y-shaped three-quark configurations, besides the standard Δ-like two-body ones. A three-body confinement potential has been shown to arise also if the quark dynamics is treated within a bag model [43]. Finally, it should be remembered that threee-body forces have been considered also in the calculations of Ref. [44] and in the relativized version of the Isgur-Karl model [3].

For a hypercentral potential the three-quark wave function is factorized,

$$\psi_{3q}(\vec{\rho},\vec{\lambda}) = \psi_{\nu\gamma}(x) Y_{[\gamma]l_\rho l_\lambda}(\Omega_\rho, \Omega_\lambda, \xi). \tag{4}$$

The hyper-radial wave function is labeled by the grand angular quantum number γ defined above and by the number of nodes ν; it is obtained as a solution of the hyper-radial equation

$$\left[\frac{d^2}{dx^2} + \frac{5}{x}\frac{d}{dx} - \frac{\gamma(\gamma+4)}{x^2}\right]\psi_{\nu\gamma}(x) = -2m[E - V_{3q}(x)]\psi_{\nu\gamma}(x). \tag{5}$$

Equation (5) can be solved analytically in two cases: The first is the six-dimensional h.o.

$$\sum_{i<j}\frac{1}{2}k(\vec{r_i}-\vec{r_j})^2 = \frac{3}{2}kx^2 = V_{\text{h.o.}}(x) \tag{6}$$

and the hyper-Coulomb (hC) potential

$$V_{\text{hC}}(x) = -\frac{\tau}{x}. \tag{7}$$

The hC term $1/x$ has important features [5,45]. First of all, the negative parity states are exactly degenerate with the first positive parity excitations. The observed Roper resonance is somewhat lower with respect to the negative parity baryon resonance, at variance with the prediction of any SU(6)-invariant two-body potential, therefore the hypercoulomb potential provides a good starting point for the description of the spectrum. Moreover, the resulting form factors have a power-law behavior, again leading to an improvement with respect to the widely used harmonic oscillator.

The hypercentral model potential includes a confinement term that is linear in x:

$$V(x) = -\frac{\tau}{x} + \alpha x. \tag{8}$$

Interactions of the linear type plus Coulomb-like type have been used for the meson sector, for example, the Cornell potential, and have been supported recently by lattice QCD calculations [46]. In this respect, the potential Eq. (8) can be considered as the hypercentral approximation of the lattice QCD potential.

The splittings within the multiplets are produced by a perturbative term breaking SU(6), which can be assumed to be the standard hyperfine interaction H_{hyp} [2]. The three-quark Hamiltonian is then

$$H = \frac{p_\lambda^2}{2m} + \frac{p_\rho^2}{2m} - \frac{\tau}{x} + \alpha x + H_{\text{hyp}}, \tag{9}$$

where m is the quark mass (taken equal to 1/3 of the nucleon mass). The strength of the hyperfine interaction is determined in order to reproduce the $\Delta - N$ mass difference, and the remaining two free parameters are fitted to the spectrum, leading to the following values [5]:

$$\alpha = 1.16\ \text{fm}^{-2}, \quad \tau = 4.59. \tag{10}$$

The spectrum given by the SU(6)-invariant part of the Hamiltoniana Eq. (9) is reported in the right part of Fig. 1. The degeneracy between the 0_S^+ and 1_M^- states, typical of the hyper-Coulomb interaction, is removed by the confinement term.

Having fixed the parameters of the potential, the hyper-radial wave functions for the ground and excited states can be calculated and therefore one can build up the three-quark states for the various resonances, taking due account of the antisymmetry requirements. In fact, the complete three-quark wave function in general can be factorized in four parts, that is, the color, spin, flavor (isospin for nonstrange baryons), and space factors:

$$\Psi_{3q} = \theta_{\text{color}} \cdot \chi_{\text{spin}} \cdot \Phi_{\text{isospin}} \cdot \psi_{3q}(\vec{\rho},\vec{\lambda}). \tag{11}$$

The color wave function must be completely antisymmetric in order to give rise to colorless baryons, and therefore the remaining factors have to be combined to an overall symmetric function.

The introduction of SU(6) configurations is beneficial, since in this way the spin and flavor states are combined to form a unique SU(6) state, which must share the same symmetry property with the space wave function. In the appendix we give the explicit form of the SU(6) configurations describing the various baryon states. Since the h.o. is a hypercentral potential as well, the SU(6) configurations are obtained by means of the same procedure followed in Ref. [2]: By simply substituting $\psi_{\nu\gamma}^{\text{h.o.}}(x)$ with $\psi_{\nu\gamma}(x)$, the eigenfunctions are obtained with the hypercentral potential of Eq. (8).

The mixing is provided by the hyperfine interaction in Eq. (9) and the mixing coefficients are obtained by fitting the observed baryon spectrum. In this way the model is completely fixed and the knowledge of the states of all resonances allows systematic calculations of various physical quantities of interest. This systematic analysis has already been performed for the photocouplings [16], the transverse electromagnetic transition amplitudes [35], the elastic nucleon form factors [20], and the ratio between the electric and magnetic proton form factors [21]. As far as the transverse electromagnetic form factors, in Ref. [35] only the negative-parity states have been considered; however, we have results for the transition to all resonances.

The three-quark interaction of Eq. (8) has been recently used in a fully relativistic approach in point form to describe the elastic electromagnetic form factors of the nucleon [23,24]

In this paper we present the parameter-free calculation of the longitudinal and transverse transition form factors using the potential of Eq. (8) with the parameters reported in Eq. (10).

III. THE HELICITY AMPLITUDES

The electromagnetic transition amplitudes, $A_{1/2}$, $A_{3/2}$, and $S_{1/2}$, are determined by the matrix elements $\mathcal{A}_{1/2}$, $\mathcal{A}_{3/2}$, $\mathcal{S}_{1/2}$ of the quark electromagnetic (e. m.) interaction, $A_\mu J^\mu$, between

TABLE I. Photocouplings (in units 10^{-3} GeV$^{-1/2}$) predicted by the hCMQ in comparison with PDG data for proton excitation to N*-like resonances. The proton transitions to the $S_{11}(1650)$, $D_{15}(1675)$, and $D_{13}(1700)$ resonances vanish in the SU(6) limit.

Resonance	$A^p_{1/2}$(hCQM)	$A^p_{1/2}$(PDG)	$A^p_{3/2}$(hCQM)	$A^p_{3/2}$(PDG)
$P_{11}(1440)$	88	-65 ± 4		
$D_{13}(1520)$	-66	-24 ± 9	67	166 ± 5
$S_{11}(1535)$	109	90 ± 30		
$S_{11}(1650)$	69	53 ± 16		
$D_{15}(1675)$	1	19 ± 8	2	15 ± 9
$F_{15}(1680)$	-35	-15 ± 6	24	133 ± 12
$D_{13}(1700)$	8	-18 ± 13	-11	-2 ± 24
$P_{11}(1710)$	43	9 ± 22		
$P_{13}(1720)$	94	18 ± 30	-17	-19 ± 20

the nucleon, N, and the resonance, B, states:

$$\mathcal{A}_{1/2} = \sqrt{\frac{2\pi\alpha}{k}}\left\langle B, J', J'_z = \frac{1}{2}\left| J_+ \right| N, J = \frac{1}{2}, J_z = -\frac{1}{2}\right\rangle,$$
$$\mathcal{A}_{3/2} = \sqrt{\frac{2\pi\alpha}{k}}\left\langle B, J', J'_z = \frac{3}{2}\left| J_+ \right| N, J = \frac{1}{2}, J_z = \frac{1}{2}\right\rangle,$$
$$\mathcal{S}_{1/2} = \sqrt{\frac{2\pi\alpha}{k}}\left\langle B, J', J'_z = \frac{1}{2}\left| J_0 \right| N, J = \frac{1}{2}, J_z = \frac{1}{2}.\right\rangle \tag{12}$$

J_μ is the electromagnetic current carried by quarks and will be used in its nonrelativistic form [13,14]; k is the virtual photon momentum in the Breit frame. For the transverse excitation, the photon has been assumed, without loss of generality, as left handed. Moreover, the z axis is assumed along the virtual photon momentum.

In order to compare the theoretical calculations with data, one has to consider that the helicity amplitudes extracted from the meson photoproduction contain also the sign of the $\pi N N^*$ vertex. The theoretical helicity amplitudes are therefore defined up to a common phase factor ζ:

$$A_{1/2,3/2} = \zeta \mathcal{A}_{1/2,3/2}, \quad S_{1/2} = \zeta \mathcal{S}_{1/2}. \tag{13}$$

The factor ζ is taken in agreement with the choice of Ref. [14], with the exception of the Roper resonance, in which case the sign is in agreement with the analysis performed in Ref. [47].

TABLE II. The same as Table I for neutron excitation.

Resonance	$A^n_{1/2}$(hCQM)	$A^n_{1/2}$(PDG)	$A^n_{3/2}$(hCQM)	$A^n_{3/2}$(PDG)
$P_{11}(1440)$	58	40 ± 10		
$D_{13}(1520)$	-1	-59 ± 9	-61	-139 ± 11
$S_{11}(1535)$	-82	-46 ± 27		
$S_{11}(1650)$	-21	-15 ± 21		
$D_{15}(1675)$	-37	-43 ± 12	-51	-58 ± 13
$F_{15}(1680)$	38	29 ± 10	15	-33 ± 9
$D_{13}(1700)$	12	0 ± 50	70	-3 ± 44
$P_{11}(1710)$	-22	-2 ± 14		
$P_{13}(1720)$	-48	1 ± 15	4	-29 ± 61

TABLE III. The same as Table I for the excitation to Δ-like resonances.

Resonance	$A^p_{1/2}$(hCQM)	$A^p_{1/2}$(PDG)	$A^p_{3/2}$(hCQM)	$A^p_{3/2}$(PDG)
$P_{33}(1232)$	-97	-135 ± 6	-169	-250 ± 8
$S_{31}(1620)$	30	27 ± 11		
$D_{33}(1700)$	81	104 ± 5	70	85 ± 2
$F_{35}(1905)$	-17	26 ± 11	-51	-45 ± 20
$F_{37}(1950)$	-28	-76 ± 12	-35	-97 ± 10

In the following we report the results of the calculations for those resonances which, according to the particle data group (PDG) classification [38], have an electromagnetic decay with three- or four-star status. This happens for twelve resonances,

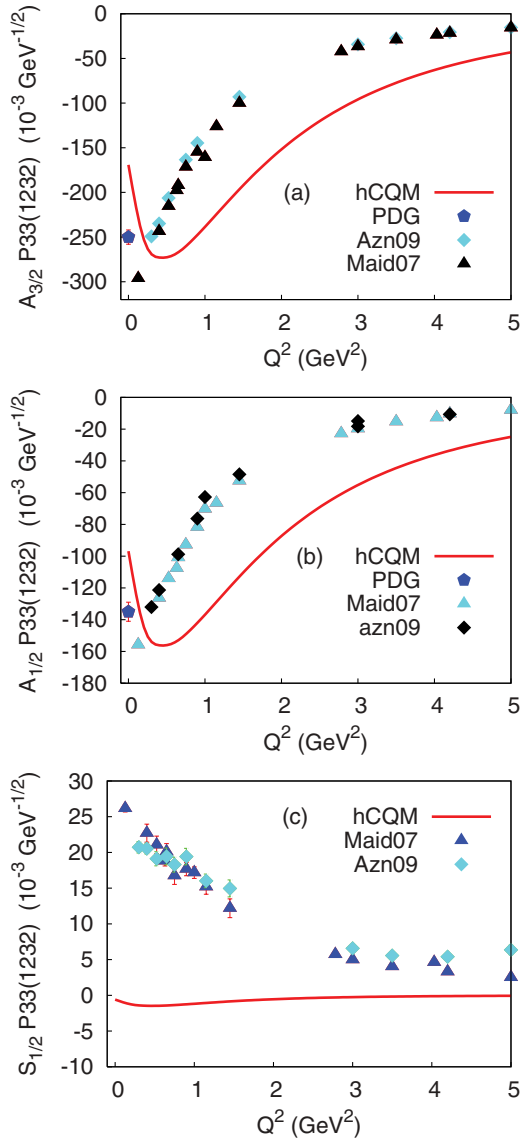

FIG. 2. (Color online) The $P_{33}(1232)$ helicity amplitudes predicted by the hCQM (full curves) $A_{3/2}$ (a), $A_{1/2}$ (b), and $S_{1/2}$ (c), in comparison with the data of Ref. [49] and with the the MAID2007 analysis [50] of the data by Refs. [51,52]. The PDG points [38] are also shown.

namely the $I = \frac{1}{2}$ states,

$$P_{11}(1440), \quad D_{13}(1520), \quad S_{11}(1535), \quad S_{11}(1650), \quad D_{15}(1675), \quad F_{15}(1680), \quad P_{11}(1710), \tag{14}$$

and the $I = \frac{3}{2}$ ones,

$$P_{33}(1232), \quad S_{31}(1620), \quad D_{33}(1700), \quad F_{35}(19005), \quad F_{37}(1950). \tag{15}$$

Besides these states, we also considered the states $D_{13}(1700)$ and $P_{13}(1720)$, which are excited in an energy range that is particularly interesting for the phenomenological analysis.

The calculations of the matrix elements of Eqs. (12) are performed using as baryon states the eigenstates of the Hamiltonian (9). For each resonance, in the appendix we list the states in the SU(6) limit; the physical states of the various resonances are given by the configuration mixing produced by the hyperfine interaction in Eq. (9).

It should be stressed that, after having fixed the free parameters [see Eq. (10)], in order to reproduce the baryon spectrum the baryon states are completely determined and the results for the helicity amplitudes reported in the following sections are parameter-free predictions of the hCQM.

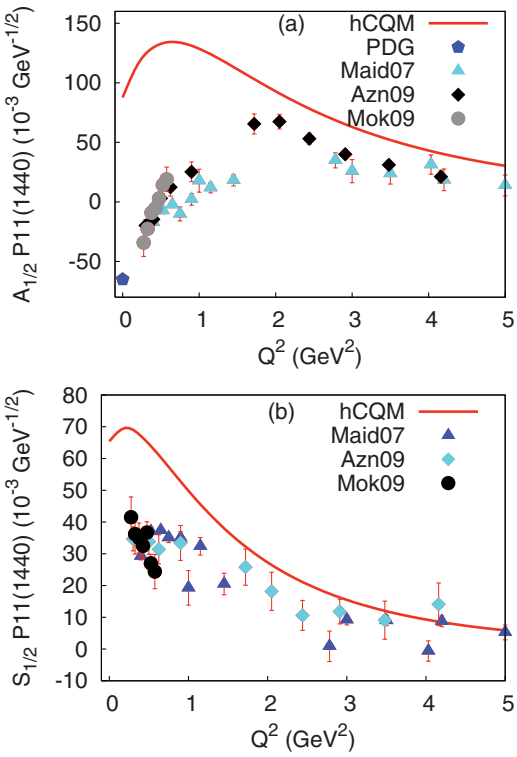

FIG. 3. (Color online) The $P_{11}(1440)$ proton transverse (a) and longitudinal (b) helicity amplitudes predicted by the hCQM (full curves), in comparison with the data of Refs. [49,60], and the MAID2007 analysis [50] of the data by Refs. [51,52,61,62]. The PDG point [38] is also shown.

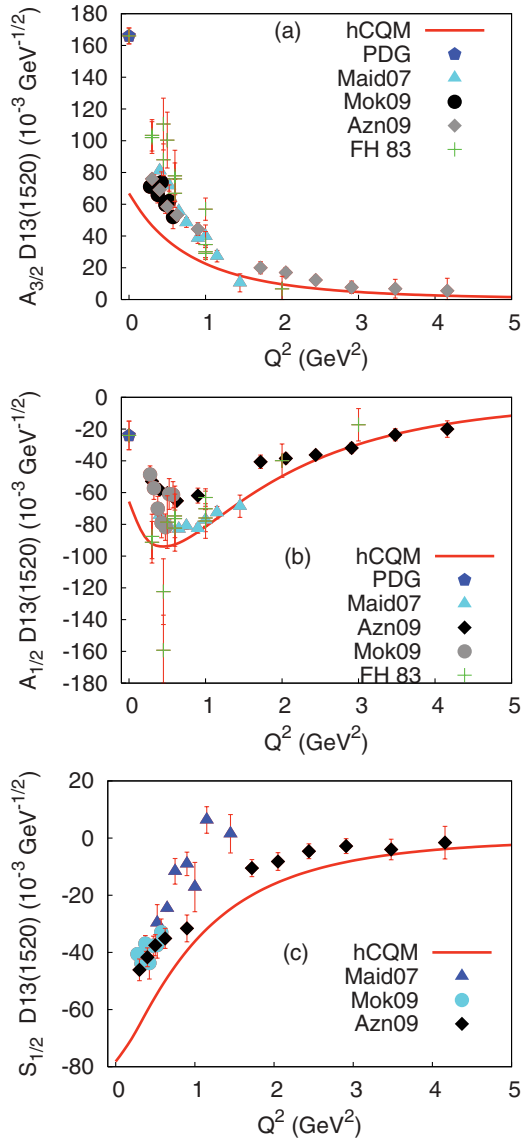

FIG. 4. (Color online) The $D_{13}(1520)$ proton helicity amplitudes predicted by the hCQM (full curves) $A_{3/2}$ (a), $A_{1/2}$ (b), and $S_{1/2}$ (c), in comparison with the data of Refs. [49,60], with the compilation reported in Refs. [65,66] and the MAID2007 analysis [50] of the data by Refs. [51,52]. The PDG points [38] are also shown.

A. The photocouplings

The proton and neutron photocouplings predicted by the hCQM [16] are reported in Tables I–III and compared with the PDG data [38]. The overall behavior is fairly well reproduced, but in general there is a lack of strength. The proton transitions to the $S_{11}(1650)$, $D_{15}(1675)$, and $D_{13}(1700)$ resonances vanish exactly in absence of hyperfine mixing and are therefore entirely due to the SU(6) violation. The results obtained with other calculations are qualitatively not much different [16,17] because the various CQM models have the same SU(6) structure in common.

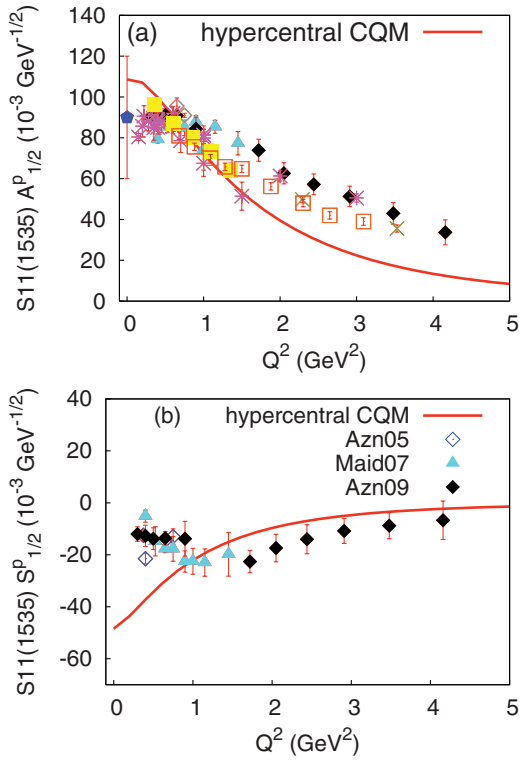

FIG. 5. (Color online) The $S_{11}(1525)$ proton transverse (a) and longitudinal (b) helicity amplitudes predicted by the hCQM (full curve), in comparison with the data of Ref. [67] (open diamonds), [49] (full diamonds), [68] (crosses), [69] (open squares), [70] (full squares), the MAID2007 analysis [50] (full triangles) of the data by Ref. [51], and the compilation of the Bonn-Mainz-DESY data of Refs. [71–74] (stars), presented in Ref. [70]. The PDG point [38] (pentagon) is also shown.

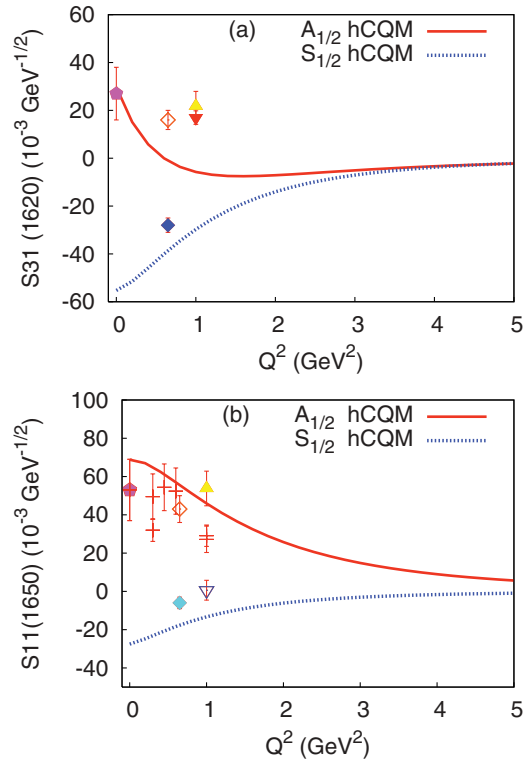

FIG. 6. (Color online) The proton helicity amplitudes predicted by the hCQM for the excitation of $S_{31}(1620)$ (a) and $S_{11}(1650)$ (b), respectively, in comparison with the data of Ref. [49] ($A_{1/2}$ open diamonds, $S_{1/2}$ full diamonds), [75] ($A_{1/2}$ open diamonds, $S_{1/2}$ full diamonds), the compilation reported in Ref. [65] and the MAID2007 analysis [50] ($A_{1/2}$ up triangles, $S_{1/2}$ down triangles) of the data in Refs. [51,52], and the compilation of the Bonn-Mainz-DESY data of Refs. [71–74] (crosses) presented in Ref. [70]. The PDG points [38] (pentagons) are also shown.

B. The transition form factors

Taking into account the Q^2 behavior of the transition matrix elements, one can calculate the hCQM helicity amplitudes [35].

In order to compare results with the experimental data, the calculation should be performed in the rest frame of the resonance (see, e.g., Ref. [48]). The nucleon and resonance wave functions are calculated in their respective rest frames and, before evaluating the matrix elements given in Eqs. (12), one should boost the nucleon to the resonance c.m.s. In our nonrelativistic approach such boost is trivial but not correct, because of the large nucleon recoil. In order to minimize the discrepancy between the nonrelativistic and the relativistic boost when comparing results with the experimental data, we use the Breit frame, as in Refs. [4,35]. Therefore we use the following kinematic relation:

$$\vec{k}^2 = Q^2 + \frac{(W^2 - M^2)^2}{2(M^2 + W^2) + Q^2}, \tag{16}$$

where M is the nucleon mass, W is the mass of the resonance, k_0 and $\vec{k}$ are the energy and the momentum of the virtual photon, respectively, and $Q^2 = \vec{k}^2 - k_0^2$. For consistency, in the calculations we have used the values of W given by the model and not the phenomenological ones.

The matrix elements of the e.m. transition operator between any two $3q$ states are expressed in terms of integrals involving the hyper-radial wave functions and are calculated numerically. The computer code has been tested by comparison with the analytical results obtained with the h.o. model of Refs. [13,14] and with the analytical model of Ref. [45].

C. The excitation to the Δ resonance

The $N - \Delta$ helicity amplitudes are shown in Fig. 2. The transverse excitation to the Δ resonance has a lack of strength at low Q^2, a feature in common with all CQM calculations. The medium-high-Q^2 behavior is decreasing too slowly with respect to data, similar to what happens for the nucleon elastic form factors [20,23]. In this case, the nonrelativistic calculations are improved by taking into account relativistic effects. Since the Δ resonance and the nucleon are in the ground state SU(6) configuration, we expect that their internal structures have strong similarities and that a good description of the $N - \Delta$ transition from factors is possible only with a relativistic approach. Such a feature is further supported by the fact that the transitions to the higher resonances are only slightly affected by relativistic effects [20].

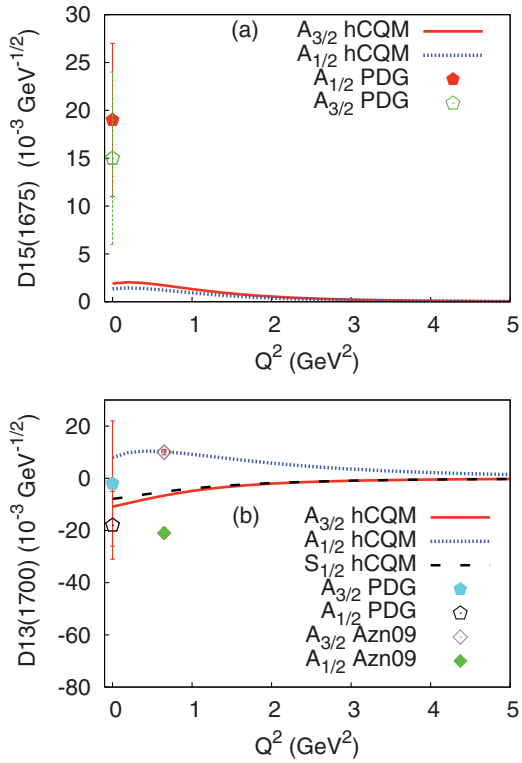

FIG. 7. (Color online) The proton helicity amplitudes predicted by the hCQM for the excitation of the $D_{15}(1675)$ (a) and $D_{13}(1700)$ (b), respectively, in comparison with the data of Ref. [49]. The PDG points [38] are also shown.

An important issue in connection with the Δ resonance is the possible deformation, which manifests itself in a nonzero value for the transverse and longitudinal quadrupole strengths. To this end one considers in particular the ratio

$$R_{EM} = -\frac{G_E}{G_M} = -\frac{\sqrt{3}A_{1/2} - A_{3/2}}{\sqrt{3}A_{1/2} + A_{3/2}}, \qquad (17)$$

where G_E and G_M are, respectively, the transverse electric and magnetic form factors for the $N \to \Delta$ transition [53]. If the quarks in the nucleon and the Δ are in a pure S-wave state there is no quadrupole excitation [54]. A deformation can be produced if the interaction contains a hyperfine term as in Eq. (9) and both the nucleon and the Δ states acquire D components.

At the photon point, the experimental value of the ratio is $R_{EM} = -0.025 \pm 0.005$ [38], which is not far from the value given by Refs. [14,55]. It should be mentioned that, by taking into account the higher shells and Siegert's theorem for a more accurate and reliable calculation, the value $R = 0.02$ was obtained [56].

In our model the ratio Eq. (17) is about 0.005, which means that the deformation is very low. This fact is confirmed by the small theoretical value of the longitudinal quadrupole transition amplitude $S_{1/2}$ [see Fig. 2 (bottom)]. As stated above, the introduction of relativity is expected to be beneficial, but the discrepancy may be due to a quite different reason.

An alternative approach to baryon resonance physics is provided by dynamical models (see, e.g., Refs. [57,58] and references therein). The calculations performed with the DMT

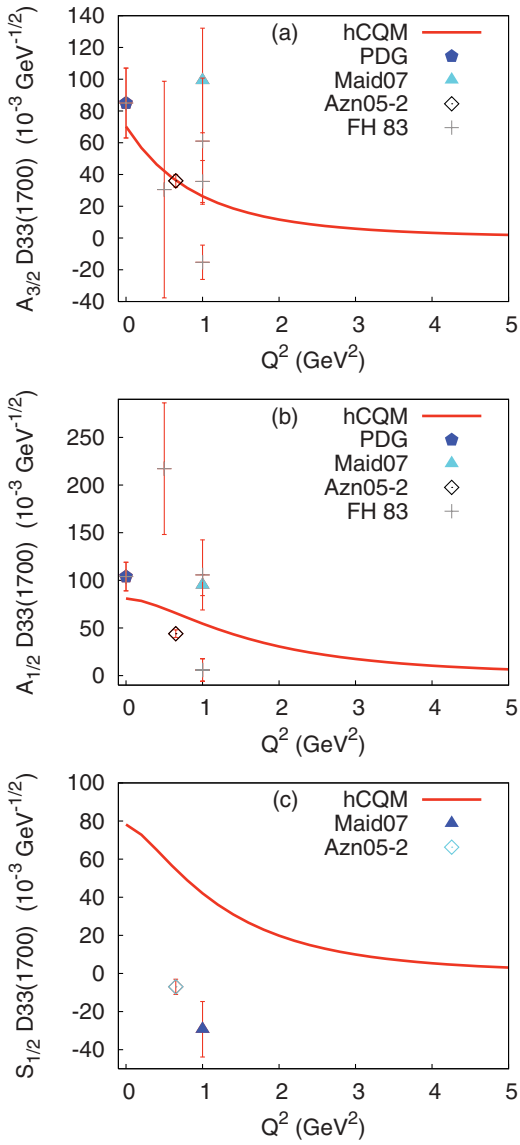

FIG. 8. (Color online) The $D_{33}(1700)$ helicity amplitudes predicted by the hCQM (full curve) $A_{3/2}$ (a), $A_{1/2}$ (b), and $S_{1/2}$ (c) in comparison with the data of Ref. [75] and the MAID2007 analysis [50] of the data by Ref. [52]. The PDG points [38] are also shown.

model [57] have shown that the $N - \Delta$ $S_{1/2}$ transition amplitude is almost completely determined by the pionic meson cloud [59]. Actually, for many other transitions, the meson cloud seems to give important contributions corresponding to the lack of strength of the hCQM [59]. This leads to the problem of missing degrees of freedom in the CQM calculations, but we come back on this topic.

D. The proton excitation to the second resonance region

1. The Roper

Because of the $\frac{1}{x}$ term in the hypercentral potential of Eq. (9), the Roper resonance can be accommodated in the first resonance region, at variance with h.o. models, which predict it to be a 2 $\hbar\omega$ state. The results for the helicity amplitudes are shown in Fig. 3. There are problems in the low-Q^2 region,

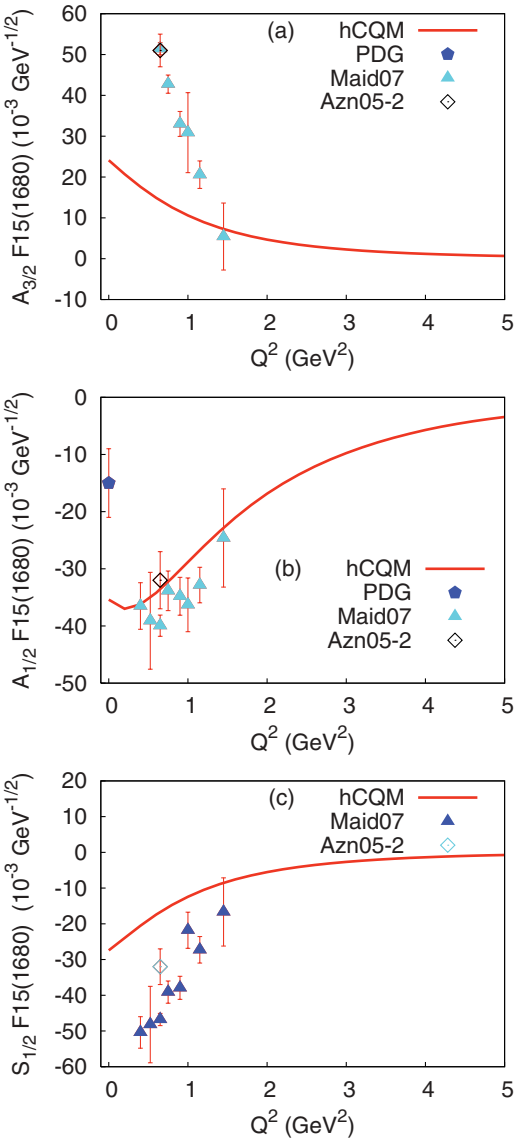

FIG. 9. (Color online) The $F_{15}(1680)$ proton helicity amplitudes predicted by the hCQM $A_{3/2}$ (a), $A_{1/2}$ (b), and $S_{1/2}$ (c), in comparison with the data of Ref. [75] and the MAID2007 analysis [50] of the data by Ref. [52]. The PDG points [38] are also shown.

but for the rest the agreement is interesting, especially if one remembers that the curves are predictions and the Roper has been often been considered a crucial state, not easily included into a constituent quark model description. In the past, exotic explanations of the Roper have been introduced; in particular, a model of the Roper as a three-quark-gluon structure has been proposed [63]. However, such model predicts a vanishing value for the longitudinal excitation [64], a result ruled out by the data shown in Fig. 3. In the present model, the Roper is a hyper-radial excitation of the nucleon.

2. *The negative-parity states*

It should be stressed that, apart from the case of the $D_{13}(1700)$ and $D_{15}(1675)$ resonances, the transverse helicity curves are the same as in Ref. [35].

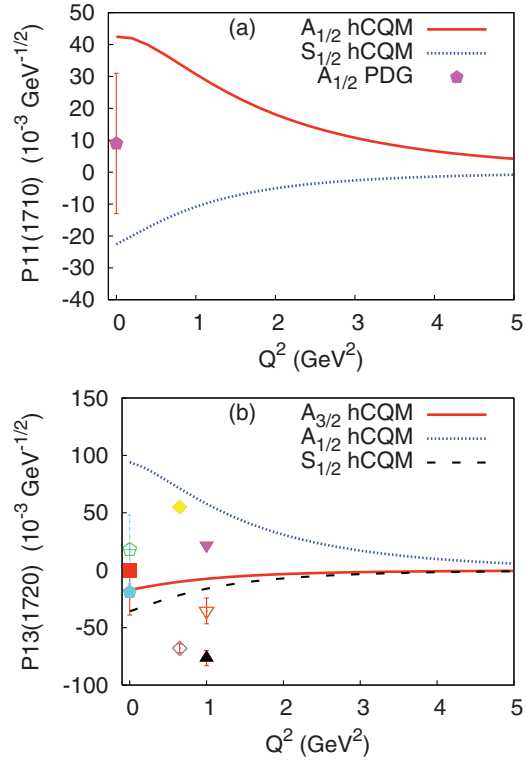

FIG. 10. (Color online) The proton helicity amplitudes predicted by the hCQM for the excitation of $P_{11}(1710)$ (a) and $P_{13}(1720)$ (b), respectively, in comparison with the data of Ref. [75] ($A_{3/2}$ open diamond, $A_{1/2}$ full diamond, $A_{3/2}$ full box) and the MAID2007 analysis [50] ($A_{3/2}$ full up triangle, $A_{1/2}$ full down triangle, $A_{3/2}$ open down triangle) of the data by Refs. [51,52]. The PDG point [38] (pentagon) is also shown.

The hCQM results for the $D_{13}(1520)$ and the $S_{11}(1535)$ resonances [35] are given in Figs. 4 and 5, respectively. The agreement in the case of the S_{11} is remarkable, the more so since the hCQM curve was published three years before the recent Jefferson Laboratory data [49,67,69,70]. In general the Q^2 behavior is reproduced, except for discrepancies at small Q^2, especially in the $A^p_{3/2}$ amplitude of the transition to the $D_{13}(1520)$ state. These discrepancies could be ascribed either to the nonrelativistic character of the model or to the lack of explicit quark-antiquark configurations, which may be important at low Q^2. The kinematical relativistic corrections at the level of boosting the nucleon and the resonance states to a common frame are not responsible for these discrepancies, as we have demonstrated in Ref. [37].

Similar results are obtained for the other negative-parity resonances (see Figs. 6, 7, and 8).

It is interesting to discuss the influence of the hyperfine mixing on the excitation of the resonances. Usually there is a very small difference between the values calculated with or without hyperfine interaction. In some cases, however the excitation strength vanishes in the SU(6) limit and the nonzero final result is entirely due to the hyperfine mixing of states. This happens for the excitation to the $S_{11}(1650)$ resonance, for both the transverse and longitudinal strengths.

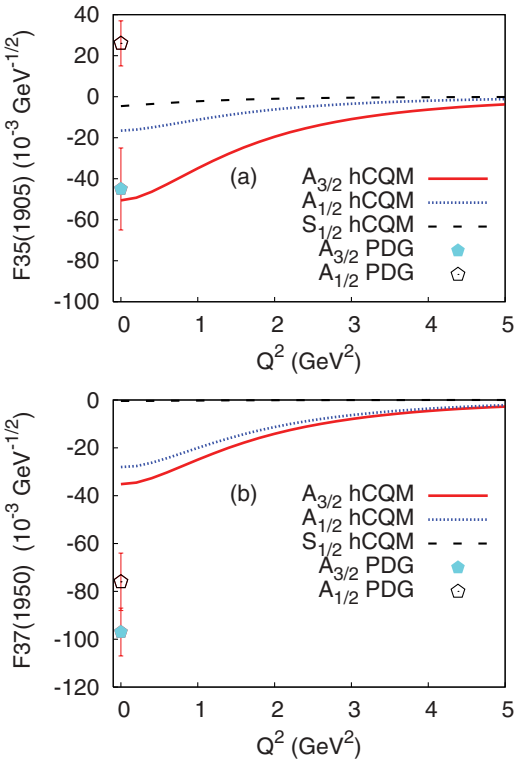

FIG. 11. (Color online) The proton helicity amplitudes predicted by the hCQM for the excitation of $F_{35}(1905)$ (a) and $F_{37}(1950)$ (b), respectively. The PDG points [38] (pentagons) are also shown.

The same thing happens for all the three helicity amplitudes of the $D_{13}(1700)$ resonance, but in this case, at variance with the $S_{11}(1650)$ state, the hyperfine mixing produces a low excitation strength. Also, in the case of the transverse excitation of the $D_{15}(1675)$, the strength is given by the hyperfine mixing, while the longitudinal amplitude $S_{1/2}$ vanishes also in presence of a SU(6) violation.

It should be mentioned that the r.m.s. radius of the proton corresponding to the parameters of Eq. (10) is 0.48 fm, which is just the value fitted in Ref. [13] to the D_{13} photocoupling. The missing strength at low Q^2 can be ascribed to the lack of quark-antiquark effects [35], probably important in the outer region of the nucleon. In this way the emerging picture in connection with the resonance excitation is that of a small confinement zone of about 0.5 fm surrounded by a sort of quark-antiquark (or meson) cloud.

For the higher negative-parity resonance, the main problem is the lack of data; however, the comparison with the hypercentral CQM does not contradict the observations made above.

E. The proton excitation to the third and fourth resonance regions

In this region the strength is dominated by the excitation to the $F_{15}(1680)$ resonance and the results calculated with the hCQM are shown in Fig. 9.

The situation is similar to that of the $D_{13}(1520)$ resonance. Here also the $A_{1/2}$ amplitude is fairly well reproduced, with

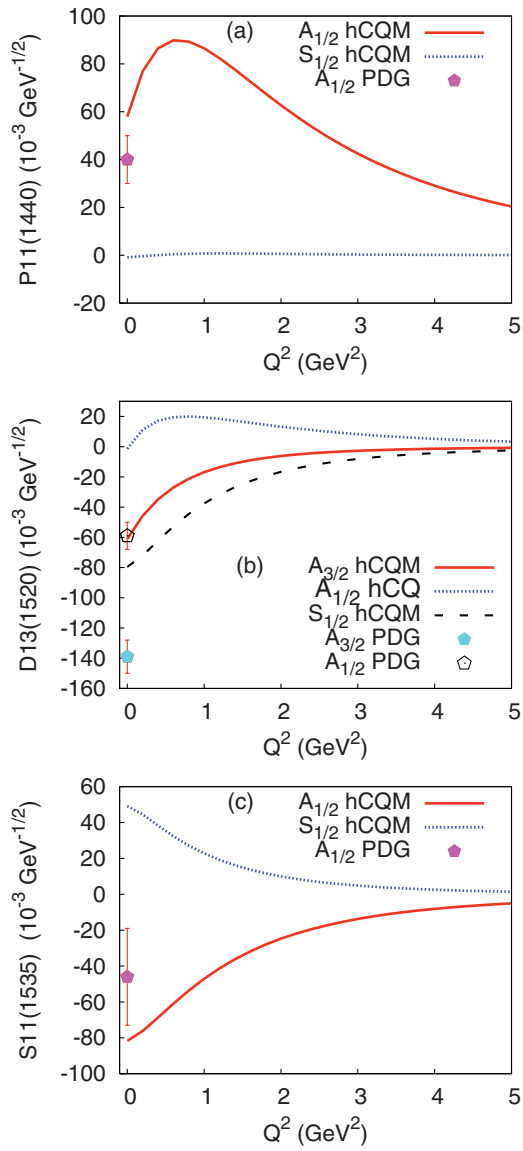

FIG. 12. (Color online) The neutron excitation strength predicted by the hypercentral CQM, in comparison with the PDG points [38] (part 1).

possibly some problem in the low-Q^2 region, while the $A_{3/2}$ amplitude exhibits a relevant lack of strength al low Q^2. For the longitudinal amplitude, there is also a lack of strength; however, new data at medium Q^2 are certainly needed.

As for the higher resonances, we note that our model predicts a second Roper-like state in the third resonance region (see Fig. 1). Performing the calculations identifying it with the state $P_{11}(1710)$, we get a relevant excitation strength [Fig. 10(a)]. The problem of a second Roper state is still open, since in some analysis there seems to be no evidence of its existence [38,76]; on the contrary, the presence of a state $P_{11}(1710)$ is supported by the recent analysis based on the Dubna-Mainz-Taipei (DMT) dynamical model [77]. In this energy region, the strength seems to be dominated by the $P_{13}(1720)$ resonance [Fig. 10(b)], for which few data up to $Q^2 = 1$ (GeV)^2 [75] are available. With these scarce data, a

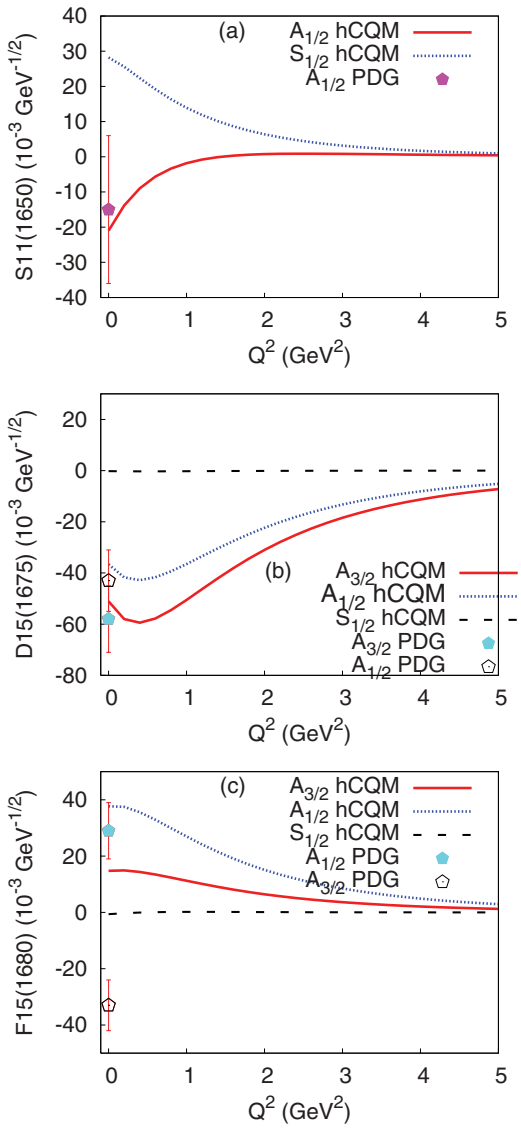

FIG. 13. (Color online) The neutron excitation strength predicted by the hypercentral CQM, in comparison with the PDG points [38] (part 2).

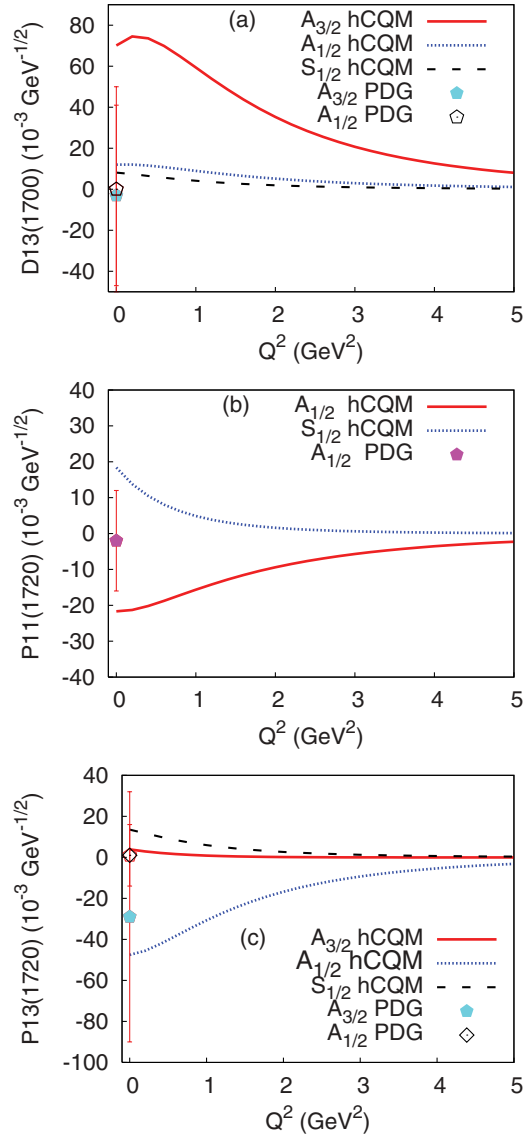

FIG. 14. (Color online) The neutron excitation strength predicted by the hypercentral CQM, in comparison with the PDG points [38] (part 3).

comparison is preliminary; however, here again there seems to be a lack of strength, especially for the $A_{3/2}$ amplitude.

In Fig. 11, the results for the remaining higher resonances $F_{35}(1905)$ and $F_{37}(1950)$ are shown. For the former, a relevant excitation strength is predicted for the $A_{3/2}$ amplitude. We hope new data will allow a reasonable comparison with the theoretical quantities.

F. The neutron excitation to the $I = \frac{1}{2}$ states

Of course, the proton and neutron excitations to the $I = \frac{3}{2}$ states are the same for isospin reasons.

In all the other cases there are both isoscalar and isovector contributions, which make the neutron strength quite different from the proton ones, as can be seen in Figs. 12, 13, and 14.

As a general observation, at least one of the neutron helicity amplitudes is not negligible. Also the longitudinal (charge) excitation is often relevant, an effect due clearly to the presence of charged particles moving within the neutron. Particularly interesting is the comparison between the two Roper resonances: for the $P_{11}(1440)$ state, the excitation is purely transverse, while the $P_{11}(1710)$ presents comparable longitudinal and transverse amplitudes, although opposite in sign.

The measurement of the neutron excitation is difficult, since one has to rely upon targets with bound neutrons, but experimental information would be highly important in order to test our knowledge on the internal nucleon structure.

IV. CONCLUSIONS

We have reported the predictions of the hCQM [5] for the transverse and longitudinal helicity amplitudes regarding the electromagnetic excitation of various baryon resonances.

The transverse excitation amplitudes to the negative-parity resonances have been already presented in Ref. [35]. The excitations chosen in this paper concern the twelve baryon resonance that, according to the PDG classification [38], exhibit a relevant photoexcitation, and the two resonances $D_{13}(1700)$ and $P_{13}(1720)$, which seem to play a relevant role in the phenomenological analyses.

The comparison between data and theoretical results suffers from the lack of experimental points for various resonances, especially at high Q^2. However, the model, even if nonrelativistic, is able to give an overall description of present data, in particular of the medium-high-Q^2 behavior of many amplitudes. At low Q^2 there is often a lack of strength, especially for the transverse $A_{3/2}$ amplitudes. We recall that the calculated proton radius provided by the model is about 0.48 fm and that a radius of this size is required for the description of the e.m. excitation to the F_{15} and D_{13} resonances [13]. The smallness of the proton radius together with the lack of strength in the low-Q^2 region suggest an interesting picture for the protons (and consequently for hadrons), namely that of a small core, with radius of about 0.5 fm, surrounded by an external quark-antiquark (or meson) cloud. The contributions coming from this external cloud have been pointed out as a possible origin of the missing strength [7,16,35] and are obviously lacking in the available CQMs. Their effect is expected to decrease for medium-high Q^2 and therefore it is not a surprise that CQMs fail to reproduce the strength at the photon point but give reasonable results for medium Q^2. These considerations are supported by the evaluation of the pion contributions performed using the Mainz-Dubna dynamical model [57], which have shown that the importance of such contributions systematically decreases with increasing Q^2, going rapidly to zero [59].

Another important issue is relativity. The present hCQM is nonrelativistic and allows us to calculate the three-quark wave function in the baryon rest frame. The e.m. form factors are evaluated in the Breit frame [see Eq. (16)], and this implies that a Lorentz transformation should to be applied to both the initial and final baryon states. This can be done quite easily [37], with the result that the helicity amplitudes are only slightly modified, probably because the high mass values of the resonances lead to a nonrelevant recoil of the three-quark states. Such situation is quite different from the elastic form factor case [20], where the simple application of Lorentz boosts is important but still not sufficient to obtain a good description of the experimental data: In fact a fully relativistic theory is needed, as in Refs. [19,23–27], which uses a relativistic Hamiltonian for the dynamics of the three-quark system. Such relativistic formulation should be extended also to the calculation of the helicity form factors (work in this direction is in progress); however, because of the above considerations, the expectation is that the calculated helicity amplitudes should not differ too much from the nonrelativistic ones and that the relativistic corrections are not responsible for the lack of strength at low Q^2.

Finally, it should be remembered that a good description of the elastic form factors in some cases is achieved only by introducing intrinsic quark form factors [19,23,24]. Presently the role of these form factors is to parametrize all those effects that are not included in the theory, namely any intrinsic structure of the constituent quarks, but also the quark-antiquark pair or meson cloud contributions. In order to investigate the role of the constituent quark structure, especially at high Q^2 [78], it would be necessary to separate the two effects. An important breakthrough in this direction is provided by recent work [79–83] in which an unquenched constituent quark model for baryons has been formulated and the quark-antiquark pair contributions to the spin and the flavor asymmetry in the proton have been calculated consistently.

The way is now open for a fully relativistic calculation of the helicity amplitudes in an unquenched CQM and a systematic study of the influence of the CQ intrinsic structure. However, the calculations presented in this paper show that, nevertheless, the CQM with a hypercentral interaction provides a reasonable basis for an overall description of the helicity amplitudes.

APPENDIX: THE BARYON STATES

The baryon states are superpositions of SU(6)−configurations, which, according to Eq. (11), can be factorized as follows:

$$\Psi_{3q} = \theta_{\text{color}} \cdot \chi_{\text{spin}} \cdot \Phi_{\text{isospin}} \cdot \psi_{3q}(\vec{\rho}, \vec{\lambda}). \tag{A1}$$

As already mentioned in the text, the various parts must be combined in order to have a completely antisymmetric three-quark wave function. To this end it is necessary to study the behavior of the different factors with respect to the permutations of three objects (that is, with respect to the group S_3). In general, any three-particle wave function belongs to one of the following symmetry types: antisymmetry (A), symmetry (S), mixed symmetry with symmetric pair (MS), and mixed symmetry with antisymmetric pair (MA).

For the color part θ_{color} one must choose the antisymmetric color singlet combination.

The three-quark spin states are defined as

$$\chi_{\text{MS}} = \left|\left[\left(\tfrac{1}{2}, \tfrac{1}{2}\right)1, \tfrac{1}{2}\right]\tfrac{1}{2}\right\rangle, \tag{A2}$$

TABLE IV. Combinations $(Y_{[\gamma]l_\rho l_\lambda})_{S_3}$ of the hyperspherical harmonics $Y_{[\gamma]l_\rho l_\lambda}$ that have definite S_3 symmetry. For simplicity of notation, in the third column we have omitted the coupling of l_ρ and l_λ to the total orbital angular momentum L. Each combination is labeled as $L^P_{S_3}$, specifying the total orbital angular momentum L, the parity P, and the symmetry type A, M, or S.

γ	$L^P_{S_3}$	$(Y_{[\gamma]l_\rho l_\lambda})_{S_3}$	S_3
0	0^+_S	$Y_{[0]00}$	S
1	1^-_M	$Y_{[1]10}$	MA
		$Y_{[1]01}$	MS
2	2^+_S	$\frac{1}{\sqrt{2}}[Y_{[2]20} + Y_{[2]02}]$	S
	2^+_M	$Y_{[2]11}$	MA
		$\frac{1}{\sqrt{2}}[Y_{[2]20} - Y_{[2]02}]$	MA
	1^+_A	$Y_{[2]11}$	A
	0^+_M	$Y_{[2]11}$	MA
		$Y_{[2]00}$	MA

TABLE V. Three-quark states with positive parity. The second, third, and fourth columns show the angular momentum, parity, and S_3 symmetry, $L^P_{S_3}$, the spin, S, and isospin, T. States are shown in the last column and are written in terms of the hyper-radial wave functions, $\psi_{\nu\gamma}$, of the hyperspherical harmonics, $(Y_{[\gamma]})_{S_3}$ of Table IV, and of the spin and isospin states.

Resonance	$L^P_{S_3}$	S	T	SU(6) configurations
P_{11}	0^+_S	$\frac{1}{2}$	$\frac{1}{2}$	$\psi_{00}Y_{[0]00}\Omega_S$
	0^+_S	$\frac{1}{2}$	$\frac{1}{2}$	$\psi_{10}Y_{[0]00}\Omega_S$
	0^+_S	$\frac{1}{2}$	$\frac{1}{2}$	$\psi_{20}Y_{[0]00}\Omega_S$
	0^+_M	$\frac{1}{2}$	$\frac{1}{2}$	$\psi_{22}\frac{1}{\sqrt{2}}[Y_{[2]00}\Omega_{\rm MS}+Y_{[2]11}\Omega_{\rm MA}]$
	2^+_M	$\frac{3}{2}$	$\frac{1}{2}$	$\psi_{22}\frac{1}{\sqrt{2}}[\frac{1}{\sqrt{2}}(Y_{[2]20}-Y_{[2]02})\phi_{\rm MS}+Y_{[2]11}\phi_{\rm MA}]\chi_{\rm S}$
P_{13}	2^+_M	$\frac{1}{2}$	$\frac{1}{2}$	$\psi_{22}\frac{1}{\sqrt{2}}[\frac{1}{\sqrt{2}}(Y_{[2]20}-Y_{[2]02})\Omega_{\rm MS}+Y_{[2]11}\Omega_{\rm MA}]$
	2^+_M	$\frac{3}{2}$	$\frac{1}{2}$	$\psi_{22}\frac{1}{\sqrt{2}}[\frac{1}{\sqrt{2}}(Y_{[2]20}-Y_{[2]02})\phi_{\rm MS}+Y_{[2]11}\phi_{\rm MA}]\chi_{\rm S}$
	0^+_M	$\frac{3}{2}$	$\frac{1}{2}$	$\psi_{22}\frac{1}{\sqrt{2}}[Y_{[2]00}\phi_{\rm MS}+Y_{[2]11}\phi_{\rm MA}]\chi_{\rm S}$
	2^+_S	$\frac{1}{2}$	$\frac{1}{2}$	$\psi_{22}\frac{1}{\sqrt{2}}[Y_{[2]20}+Y_{[2]02}]\Omega_{\rm S}$
F_{15}	2^+_M	$\frac{1}{2}$	$\frac{1}{2}$	$\psi_{22}\frac{1}{\sqrt{2}}[\frac{1}{\sqrt{2}}(Y_{[2]20}-Y_{[2]02})\Omega_{\rm MS}+Y_{[2]11}\Omega_{\rm MA}]$
	2^+_M	$\frac{3}{2}$	$\frac{1}{2}$	$\psi_{22}\frac{1}{\sqrt{2}}[\frac{1}{\sqrt{2}}(Y_{[2]20}-Y_{[2]02})\phi_{\rm MS}+Y_{[2]11}\phi_{\rm MA}]\chi_{\rm S}$
	2^+_S	$\frac{1}{2}$	$\frac{1}{2}$	$\psi_{22}\frac{1}{\sqrt{2}}[Y_{[2]20}+Y_{[2]02}]\Omega_{\rm S}$
F_{17}	2^+_M	$\frac{3}{2}$	$\frac{1}{2}$	$\psi_{22}\frac{1}{\sqrt{2}}[\frac{1}{\sqrt{2}}(Y_{[2]20}-Y_{[2]02})\phi_{\rm MS}+Y_{[2]11}\phi_{\rm MA}]\chi_{\rm S}$
P_{31}	2^+_S	$\frac{3}{2}$	$\frac{3}{2}$	$\psi_{22}\frac{1}{\sqrt{2}}[(Y_{[2]20}+Y_{[2]02}]\chi_{\rm S}\phi_{\rm S}$
	0^+_M	$\frac{1}{2}$	$\frac{3}{2}$	$\psi_{22}\frac{1}{\sqrt{2}}[Y_{[2]00}\chi_{\rm MS}+Y_{[2]11}\chi_{\rm MA}]\phi_{\rm S}$
P_{33}	0^+_S	$\frac{3}{2}$	$\frac{3}{2}$	$\psi_{00}Y_{[0]00}\chi_{\rm S}\phi_{\rm S}$
	0^+_S	$\frac{3}{2}$	$\frac{3}{2}$	$\psi_{10}Y_{[0]00}\chi_{\rm S}\phi_{\rm S}$
	0^+_S	$\frac{3}{2}$	$\frac{3}{2}$	$\psi_{20}Y_{[0]00}\chi_{\rm S}\phi_{\rm S}$
	2^+_S	$\frac{3}{2}$	$\frac{3}{2}$	$\psi_{22}\frac{1}{\sqrt{2}}[Y_{[2]20}+Y_{[2]02}]\chi_{\rm S}\phi_{\rm S}$
	2^+_M	$\frac{1}{2}$	$\frac{3}{2}$	$\psi_{22}\frac{1}{\sqrt{2}}[\frac{1}{\sqrt{2}}(Y_{[2]20}-Y_{[2]02})\chi_{\rm MS}+Y_{[2]11}\chi_{\rm MA}]\phi_{\rm S}$
F_{35}	2^+_M	$\frac{1}{2}$	$\frac{3}{2}$	$\psi_{22}\frac{1}{\sqrt{2}}[\frac{1}{\sqrt{2}}(Y_{[2]20}-Y_{[2]02})\chi_{\rm MS}+Y_{[2]11}\chi_{\rm MA}]\phi_{\rm S}$
	2^+_S	$\frac{3}{2}$	$\frac{3}{2}$	$\psi_{22}\frac{1}{\sqrt{2}}[Y_{[2]20}+Y_{[2]02}]\chi_{\rm S}\phi_{\rm S}$
F_{37}	2^+_S	$\frac{3}{2}$	$\frac{3}{2}$	$\psi_{22}\frac{1}{\sqrt{2}}[Y_{[2]20}+Y_{[2]02}]\chi_{\rm S}\phi_{\rm S}$

$$\chi_{\rm MA} = \left|\left[\left(\tfrac{1}{2},\tfrac{1}{2}\right)0,\tfrac{1}{2}\right]\tfrac{1}{2}\right\rangle, \tag{A3}$$

$$\chi_{\rm S} = \left|\left[\left(\tfrac{1}{2},\tfrac{1}{2}\right)1,\tfrac{1}{2}\right]\tfrac{3}{2}\right\rangle, \tag{A4}$$

The antisymmetric combination is absent because there are only two states at disposal for three particles.

Similarly one can define the isospin states $\phi_{\rm MS}$, $\phi_{\rm MA}$, and $\phi_{\rm S}$.

If the interaction is spin and isospin (flavor) independent, one has to introduce products of $\chi-$ and $\phi-$ states with definite S_3- symmetry. Here we give the explicit forms only for the case that both factors have mixed symmetry, the remaining ones being trivial:

TABLE VI. Three-quark states with negative parity. Notation as in Table V.

Resonances	$L^P_{S_3}$	S	T	States
S_{11}	1^-_M	$\frac{1}{2}$	$\frac{1}{2}$	$\psi_{11}\frac{1}{\sqrt{2}}[Y_{[1]10}\Omega_{\rm MA}+Y_{[1]01}\Omega_{\rm MS}]$
	1^-_M	$\frac{1}{2}$	$\frac{1}{2}$	$\psi_{21}\frac{1}{\sqrt{2}}[Y_{[1]10}\Omega_{\rm MA}+Y_{[1]01}]\Omega_{\rm MS}$
	1^-_M	$\frac{3}{2}$	$\frac{1}{2}$	$\psi_{11}\frac{1}{\sqrt{2}}[Y_{[1]10}\phi_{\rm MA}+Y_{[1]01}\phi_{\rm MS}]\chi_{\rm S}$
	1^-_M	$\frac{3}{2}$	$\frac{1}{2}$	$\psi_{21}\frac{1}{\sqrt{2}}[Y_{[1]10}\phi_{\rm MA}+Y_{[1]01}\phi_{\rm MS}]\chi_{\rm S}$
D_{13}	1^-_M	$\frac{1}{2}$	$\frac{1}{2}$	$\psi_{11}\frac{1}{\sqrt{2}}[Y_{[1]10}\Omega_{\rm MA}+Y_{[1]01}\Omega_{\rm MS}]$
	1^-_M	$\frac{1}{2}$	$\frac{1}{2}$	$\psi_{21}\frac{1}{\sqrt{2}}[Y_{[1]10}\Omega_{\rm MA}+Y_{[1]01}]\Omega_{\rm MS}$
	1^-_M	$\frac{3}{2}$	$\frac{1}{2}$	$\psi_{11}\frac{1}{\sqrt{2}}[Y_{[1]10}\phi_{\rm MA}+Y_{[1]01}\phi_{\rm MS}]\chi_{\rm S}$
	1^-_M	$\frac{3}{2}$	$\frac{1}{2}$	$\psi_{21}\frac{1}{\sqrt{2}}[Y_{[1]10}\phi_{\rm MA}+Y_{[1]01}\phi_{\rm MS}]\chi_{\rm S}$
D_{15}	1^-_M	$\frac{3}{2}$	$\frac{1}{2}$	$\psi_{11}\frac{1}{\sqrt{2}}[Y_{[1]10}\phi_{\rm MA}+Y_{[1]01}\phi_{\rm MS}]\chi_{\rm S}$
	1^-_M	$\frac{3}{2}$	$\frac{1}{2}$	$\psi_{21}\frac{1}{\sqrt{2}}[Y_{[1]10}\phi_{\rm MA}+Y_{[1]01}\phi_{\rm MS}]\chi_{\rm S}$
S_{31}	1^-_M	$\frac{1}{2}$	$\frac{3}{2}$	$\psi_{11}\frac{1}{\sqrt{2}}[Y_{[1]10}\chi_{\rm MA}+Y_{[1]01}\chi_{\rm MS}]\phi_{\rm S}$
	1^-_M	$\frac{1}{2}$	$\frac{3}{2}$	$\psi_{21}\frac{1}{\sqrt{2}}[Y_{[1]10}\chi_{\rm MA}+Y_{[1]01}\chi_{\rm MS}]\phi_{\rm S}$
S_{33}	1^-_M	$\frac{1}{2}$	$\frac{3}{2}$	$\psi_{11}\frac{1}{\sqrt{2}}[Y_{[1]10}\chi_{\rm MA}+Y_{[1]01}\chi_{\rm MS}]\phi_{\rm S}$
	1^-_M	$\frac{1}{2}$	$\frac{3}{2}$	$\psi_{21}\frac{1}{\sqrt{2}}[Y_{[1]10}\chi_{\rm MA}+Y_{[1]01}\chi_{\rm MS}]\phi_{\rm S}$

$$\Omega_{\rm S} = \frac{1}{\sqrt{2}}[\chi_{\rm MA}\phi_{\rm MA}+\chi_{\rm MS}\phi_{\rm MS}], \tag{A5}$$

$$\Omega_{\rm MS} = \frac{1}{\sqrt{2}}[\chi_{\rm MA}\phi_{\rm MA}-\chi_{\rm MS}\phi_{\rm MS}], \tag{A6}$$

$$\Omega_{\rm MA} = \frac{1}{\sqrt{2}}[\chi_{\rm MA}\phi_{\rm MS}+\chi_{\rm MS}\phi_{\rm MA}], \tag{A7}$$

$$\Omega_A = \frac{1}{\sqrt{2}}[\chi_{\rm MA}\phi_{\rm MS}-\chi_{\rm MS}\phi_{\rm MA}], \tag{A8}$$

The symmetry properties of the space wave function

$$\psi_{3q}(\vec{\rho},\vec{\lambda}) = \psi_{\nu\gamma}(x)Y_{[\gamma]l_\rho l_\lambda}(\Omega_\rho,\Omega_\lambda,\xi) \tag{A9}$$

are determined by the hyperspherical part only, since the hyperradius x is completely symmetric. In Table IV we report the combinations of the hyperspherical harmonics having definite S_3 symmetry.

In Tables V and VI, we give the explicit form of the three-quark states with positive and negative parities, respectively. In these tables the hyper-radial wave functions $\psi_{\nu\gamma}$ are solutions of the hyper-radial equation (5); their form depends of course on the hypercentral potential.

[1] G. Morpurgo, Physics **2**, 95 (1965).
[2] N. Isgur and G. Karl, Phys. Rev. D **18**, 4187 (1978); **19**, 2653 (1979); **20**, 1191 (1979).
[3] S. Capstick and N. Isgur, Phys. Rev. D **34**, 2809 (1986).
[4] R. Bijker, F. Iachello, and A. Leviatan, Ann. Phys. (NY) **236**, 69 (1994).
[5] M. Ferraris, M. M. Giannini, M. Pizzo, E. Santopinto, and L. Tiator, Phys. Lett. B **364**, 231 (1995).
[6] M. M. Giannini, Nuovo Cimento A **76**, 455 (1983).
[7] E. Santopinto, Ph.D. thesis, Genova, 1995 (unpublished).
[8] L. Ya. Glozman and D. O. Riska, Phys. Rep. **268**, 263 (1996).

[9] L. Ya. Glozman, Z. Papp, W. Plessas, K. Varga, and R. F. Wagenbrunn, Phys. Rev. C **57**, 3406 (1998); L. Ya. Glozman, W. Plessas, K. Varga, and R. F. Wagenbrunn, Phys. Rev. D **58**, 094030 (1998).

[10] U. Löring, K. Kretzschmar, B. Ch. Metsch, and H. R. Petry, Eur. Phys. J. A **10**, 309 (2001); U. Löring, B. Ch. Metsch, and H. R. Petry, *ibid.* **10**, 395 (2001); **10**, 447 (2001).

[11] K. Wilson, Phys. Rev. D **10**, 2445 (1974); J. Kogut and L. Susskind, *ibid.* **9**, 3501 (1974).

[12] A. De Rújula, H. Georgi, and S. L. Glashow, Phys. Rev. D **12**, 147 (1975).

[13] L. A. Copley, G. Karl, and E. Obryk, Phys. Lett. **29**, 117 (1969).

[14] R. Koniuk and N. Isgur, Phys. Rev. D **21**, 1868 (1980).

[15] S. Capstick, Phys. Rev. D **46**, 2864 (1992).

[16] M. Aiello, M. Ferraris, M. M. Giannini, M. Pizzo, and E. Santopinto, Phys. Lett. B **387**, 215 (1996).

[17] S. Capstick and W. Roberts, Prog. Part. Nucl. Phys. **45**, 241 (2000).

[18] R. Bijker, F. Iachello, and A. Leviatan, Phys. Rev. C **54**, 1935 (1996).

[19] F. Cardarelli, E. Pace, G. Salmè, and S. Simula, Phys. Lett. B **357**, 267 (1995); F. Cardarelli and S. Simula, Phys. Rev. C **62**, 065201 (2000).

[20] M. De Sanctis, E. Santopinto, and M. M. Giannini, Eur. Phys. J. A **1**, 187 (1998).

[21] M. De Sanctis, M. M. Giannini, L. Repetto, and E. Santopinto, Phys. Rev. C **62**, 025208 (2000).

[22] M. K. Jones *et al.* (The Jefferson Lab. Hall A. Collaboration), Phys. Rev. Lett. **84**, 1398 (2000); O. Gayou *et al.*, Phys. Rev. C **64**, 038202 (2001); O. Gayou *et al.* (Jefferson Lab. Hall A. Collaboration), Phys. Rev. Lett. **88**, 092301 (2002); B. D. Milbrath *et al.* (Bates FPP Collaboration), *ibid.* **80**, 452 (1998); **82**, 2221(E) (1999); T. Pospischil *et al.* (A1 Collaboration), Eur. Phys. J. A **12**, 125 (2001); V. Punjabi *et al.*, Phys. Rev. C **71**, 055202 (2005).

[23] M. De Sanctis, M. M. Giannini, E. Santopinto, and A. Vassallo, Phys. Rev. C **76**, 062201(R) (2007); Nucl. Phys. A **782**, 57 (2007); **755**, 294 (2005); Eur. Phys. J. **19**, 81 (2004); M. M. Giannini, E. Santopinto, and A. Vassallo, Nucl. Phys. A **699**, 308 (2002); D. Y. Chen, Y. B. Dong, M. M. Giannini, and E. Santopinto, *ibid.* **782**, 62 (2007).

[24] E. Santopinto, A. Vassallo, M. M. Giannini, and M. De Sanctis, Phys. Rev. C **82**, 065204 (2010).

[25] R. F. Wagenbrunn, S. Boffi, W. Klink, W. Plessas, and M. Radici, Phys. Lett. B **511**, 33 (2001).

[26] S. Boffi, L. Y. Glozman, W. Klink, W. Plessas, M. Radici, and R. F. Wagenbrunn, Eur. Phys. J. A **14**, 17 (2002).

[27] D. Merten, U. Loring, K. Kretzschmar, B. Metsch, and H. R. Petry, Eur. Phys. J. A **14**, 477 (2002).

[28] F. E. Close and Z. Li, Phys. Rev. D **42**, 2194 (1990); **42**, 2207 (1990).

[29] M. Warns, H. Schroder, W. Pfeil, and H. Rollnik, Z. Phys. C **45**, 613 (1990); **45**, 627 (1990).

[30] R. H. Stanley and H. J. Weber, Phys. Rev. C **52**, 435 (1995).

[31] S. Capstick and B. D. Keister, Phys. Rev. D **51**, 3598 (1995).

[32] F. Cardarelli, E. Pace, G. Salmè, and S. Simula, Phys. Lett. B **371**, 7 (1996).

[33] F. Cardarelli, E. Pace, G. Salmè, and S. Simula, Phys. Lett. B **397**, 13 (1997).

[34] I. G. Aznauryan and V. D. Burkert, Phys. Rev. C **85**, 055202 (2012).

[35] M. Aiello, M. M. Giannini, and E. Santopinto, J. Phys. G: Nucl. Part. Phys. **24**, 753 (1998).

[36] Seventh European Research Conference on Electromagnetic Interactions with Nucleons and Nuclei (EINN 2007), Milos Island, Greece, 2007 (unpublished); BRAG Meeting, Bonn, 2007 (unpublished); Electromagnetic N-N* Transition Form Factors Workshop, Jlab, Newport News, 2008 (unpublished); Hadron Electromagnetic Form Factors, ECT*, Trento, 2008 (unpublished); Fifth International Pion-Nucleon PWA Workshop and Interpretation of Baryon Resonances, ECT*, Trento, 2009 (unpublished); QCD from the Bound-State Perspective, ECT*, Trento, 2010 (unpublished); Nucleon Resonance Structure in Exclusive Electroproduction at High Photon Virtualities with the CLAS 12 Detector, Jefferson Lab, 2011 (unpublished); Sixth International Pion-Nucleon PWA Workshop and Interpretation of Baryon Resonances, George Washington University, 2011 (unpublished).

[37] M. De Sanctis, E. Santopinto, and M. M. Giannini, Eur. Phys. J. A **2**, 403 (1998).

[38] K. Nakamura *et al.* (Particle Data Group), J. Phys. G: Nucl. Part. Phys. **37**, 075021 (2010).

[39] J. Ballot and M. Fabre de la Ripelle, Ann. Phys. (NY) **127**, 62 (1980).

[40] P. Hasenfratz, R. R. Horgan, J. Kuti, and J. M. Richard, Phys. Lett. B **94**, 401 (1980).

[41] M. Fabre de la Ripelle and J. Navarro, Ann. Phys. (NY) **123**, 185 (1979).

[42] N. Isgur and J. Paton, Phys. Lett. B **124**, 247 (1983); Phys. Rev. D **31**, 2910 (1985).

[43] L. Heller, in *Quarks and Nuclear Forces*, edited by D. C. Vries and B. Zeitnitz, Springer Tracts Mod. Phys., Vol. 100 (Springer, New York, 1982).

[44] J. Carlson, J. Kogut, and V. R. Pandharipande, Phys. Rev. D **27**, 233 (1983).

[45] E. Santopinto, F. Iachello, and M. M. Giannini, Nucl. Phys. A **623**, 100C (1997); Eur. Phys. J. A **1**, 307 (1998); R. Bijker, F. Iachello, and E. Santopinto, J. Phys. A **31**, 9041 (1998).

[46] G. S. Bali, C. Schlichter, and K. Schilling, Phys. Rev. D **51**, 5165 (1995).

[47] I. G. Aznauryan, Phys. Rev. C **76**, 025212 (2007).

[48] I. G. Aznauryan and V. Burkert, Prog. Nucl. Part. Phys. **67**, 1 (2012).

[49] I. G. Aznauryan *et al.* (CLAS Collaboration), Phys. Rev. C **80**, 055203 (2009).

[50] D. Drechsel, S. S. Kamalov, and L. Tiator, Eur. Phys. J. A **34**, 69 (2007).

[51] K. Joo *et al.* (JLab-CLAS Collaboration), Phys. Rev. Lett. **88**, 122001 (2002).

[52] G. Laveissière *et al.* (JLab-Hall A Collaboration), Phys. Rev. C **69**, 045203 (2004).

[53] R. C. Devenish, T. S. Eisenschitz, and J. G. Koerner, Phys. Rev. D **14**, 3063 (1976).

[54] C. M. Becchi and G. Morpurgo, Phys. Lett. **17**, 352 (1965).

[55] N. Isgur, G. Karl, and R. Koniuk, Phys. Rev. D **25**, 2394 (1982).

[56] D. Drechsel and M. M. Giannini, Phys. Lett. B **143**, 329 (1984).

[57] S. S. Kamalov, S. N. Yang, D. Drechsel, O. Hanstein, and L. Tiator, Phys. Rev. C **64**, 032201 (2001).

[58] T. Sato and T. S. H. Lee, Phys. Rev. C **63**, 055201 (2001).

[59] L. Tiator, D. Drechsel, S. Kamalov, M. M. Giannini, E. Santopinto, and A. Vassallo, Eur. Phys. J. A **19**, 55 (2004).

[60] V. I. Mokeev, V. D. Burkert, T.-S. H. Lee, L. Elouadrhiri, G. V. Fedotov, and B. S. Ishkhanov (CLAS Collaboration), Phys. Rev. C **80**, 045212 (2009).
[61] V. V. Frolov *et al.* (JLab-Hall C Collaboration), Phys. Rev. Lett. **82**, 45 (1999).
[62] M. Ungaro *et al.* (JLab-CLAS Collaboration), Phys. Rev. Lett. **C 97**, 112003 (2006).
[63] Z. P. Li, Phys. Rev. D **44**, 2841 (1991); Z. P. Li, V. Burkert, and Zh. Li, *ibid.* **46**, 70 (1992).
[64] I. G. Aznauryan *et al.* (CLAS Collaboration), Phys. Rev. C **78**, 045209 (2008).
[65] F. Foster and G. Hughes, Rep. Prog. Phys. **46**, 1445 (1983).
[66] Ch. Gerhardt, Z. Phys. C **4**, 311 (1980).
[67] I. G. Aznauryan, V. D. Burkert, H. Egiyan, K. Joo, R. Minehart, and L. C. Smith, Phys. Rev. C **71**, 015201 (2005).
[68] C. S. Armstrong *et al.*, Phys. Rev. D **60**, 052004 (1999).
[69] H. Denizli *et al.* (CLAS Collaboration), Phys. Rev. C **76**, 015204 (2007).
[70] R. Thompson *et al.* (CLAS Collaboration), Phys. Rev. Lett. **86**, 1702 (2001).
[71] B. Krusche *et al.*, Phys. Rev. Lett. **74**, 3736 (1995).
[72] F. W. Brasse *et al.*, Nucl. Phys. B **139**, 37 (1978); Z. Phys. C **22**, 33 (1984).
[73] U. Beck *et al.*, Phys. Lett. B **51**, 103 (1974).
[74] H. Breuker *et al.*, Phys. Lett. B **74**, 409 (1978).
[75] I. G. Aznauryan, V. D. Burkert, G. V. Fedotov, B. S. Ishkhanov, and V. I. Mokeev, Phys. Rev. C **72**, 045201 (2005).
[76] R. A. Arndt, W. J. Briscoe, I. I. Strakovsky, and R. L. Workman, Phys. Rev. C **74**, 045205 (2006).
[77] S. N. Yang, S. Kamalov, and L. Tiator, AIP Conf. Proc. **1432**, 293 (2012).
[78] Aznauryan, V. Braun, V. Burkert, S. Capstick, R. Edwards, I. C. Cloet, M. Giannini, T.-S. H. Lee, H.-W. Lin, V. Mokeev, C. D. Roberts, E. Santopinto, P. Stoler, Q. Zhao, and B. Zou, JLAB-PHY-09-993 (2009) (unpublished); S. Capstick, A. Svarc, L. Tiator, J. Gegelia, M. M. Giannini, E. Santopinto, C. Hanhart, S. Scherer, T.-S. H. Lee, T. Sato, and N. Suzuki, Eur. Phys. J. A **35**, 253 (2008).
[79] E. Santopinto and R. Bijker, Few-Body Syst. **44**, 95 (2008).
[80] R. Bijker and E. Santopinto, Phys. Rev. C **80**, 065210 (2009).
[81] E. Santopinto and R. Bijker, Phys. Rev. C **82**, 062202 (2010).
[82] E. Santopinto, R. Bijker, and J. Ferretti, Few-Body Syst. **50**, 199 (2011).
[83] R. Bijker, J. Ferretti, and E. Santopinto, Phys. Rev. C **85**, 035204 (2012).